Available online at www.sciencedirect.com
ScienceDirect
Journal of Hazardous Materials 147 (2007) 738–745
Journal of Hazardous Materials
www.elsevier.com/locate/jhazmat

Dynamic sorption of ionizable organic compounds (IOCs) and xylene from water using geomaterial-modified montmorillonite

M. Houari [a], B. Hamdi [b], J. Brendle [c], O. Bouras [a], J.C. Bollinger [d], M. Baudu [d,*]

[a] *Departement of Chemical Engineering, University of Blida, P.O. Box 270-09000 Blida, Algeria*
[b] *Laboratoire LEPCMAE, Faculté de Chimie, USTHB, BP 32 El Alia, 16111 Alger, Algeria*
[c] *Laboratoire des Matériaux à Porosité Contrôlée, ENSC Mulhouse, 3 Rue Alfred Werner, Mulhouse Cedex, France*
[d] *Laboratoire LSEE, Faculté des Sciences et Techniques, 123 Avenue Albert Thomas, F-87060 Limoges Cedex, France*

Received 4 October 2006; received in revised form 16 January 2007; accepted 17 January 2007
Available online 3 February 2007

Abstract

Adsorption of phenols and xylene onto composite material, Na-montmorillonite, activated carbon, cement and water mixture, 70%, 7%, 7% and 16% (w/w/w/w), respectively, was studied at pH values of 5.15, 4.55, 5.2 and 4.9, respectively, of phenol, 2-CP, 2-NP and xylene. Equilibrium isotherms and fixed-bed column studies were undertaken to evaluate the performance of clay-active coal-coated cement (CACC) in removing phenols from aqueous solution.

Investigations revealed CACC to be a very efficient media for the removal of phenols from water. The suitability of the Langmuir adsorption model to the equilibrium data was investigated for all phenols–adsorbent systems. At the maximum sorption capacity of the composite material it was found that the uptake (mg phenols/g) of phenols increased in the order 2-CP > 2-NP > phenol ∼ *m*-xylene as do their solubilities. The LUB design approach was used to determine the equivalent length of unused bed. The lower LUB values imply a better utilization of CACC composite. A model, which considered the effect of axial dispersion, was successfully used to describe the fixed-bed operation, the axial dispersion coefficient increased significantly with solubility.

Keywords: Montmorillonite; Geomaterial; Isotherm; Breakthrough curve; Phenols

1. Introduction

Phenolic compounds are considered to be hazardous wastes that are released into the aquatic environment by industries such as coke ovens in steel plants, petroleum refineries, petrochemical, phenolic resin, fertilizer, pharmaceutical, chemical, and dye industries and have been reported in hazardous wastes sites. The literature reports many studies concerning the optimization of adsorption onto new adsorbent products and elucidating the mechanism of the process [1–3]. This study concerns the applicability of bentonite as an alternative adsorbent for the removal of substituted phenols [4–6].

Clays are widely used as adsorbents due to their high specific surface area. On the other hand, their sorption capacity is very low for organic molecules that are highly water soluble, polar, or cationic. This is due to the hydrophilic nature of the mineral surfaces. Natural clay has a negative charge that is compensated by exchangeable cations, such as Na^+ and Ca^{2+} on their surfaces.

Over the last 20 years, several studies have been carried out on the use of quaternary ammonium salt exchanged clays (QASCs) as adsorbents of many organic compounds from water, as well as on their application as pre-solidification agents in cement-based stabilization processes [7,8]. Furthermore, patents have been filed using QASCs as adsorbents in view of their application in waste disposal [9,10]. The use of QASCs as pre-solidification agents in cement-based stabilization of organic-containing wastes relies on the high adsorption power of these clays and their compatibility with the cementations matrix [11].

In previous work, Montgomery et al. [12] carried out a microstructural study using scanning electron microscopy (SEM) and X-ray diffraction analysis (XRD) of solid mixes of QASCs containing organics and ordinary portland cement

* Corresponding author. Tel.: +33 5 55 45 72 04; fax: +33 5 55 45 72 03.
E-mail address: michel.baudu@unilim.fr (M. Baudu).

0304-3894/$ – see front matter © 2007 Elsevier B.V. All rights reserved.
doi:10.1016/j.jhazmat.2007.01.113

Nomenclature

a	mass transfer area per unit volume (m^2/m^3)
C_e	liquid-phase sorbate concentration in equilibrium with q (M)
C_F	feed sorbate concentration (M)
d_p	clay particle size (cm)
D_c	column diameter (cm)
D_e	effective diffusivity within clay particle (m^2/s)
D_L	liquid-phase diffusivity (m^2/s)
k_L	individual liquid-film mass transfer coefficient (cm/h)
K_1	Langmuir constant (M^{-1})
K_L	overall liquid-phase mass transfer coefficient (cm/h)
L	bed height (cm)
q	solid-phase sorbate concentration (mmol/g)
q_m	solid-phase sorbate concentration corresponding to complete coverage (mmol/g)
t	contact time (min)
$t_{1/2}$	time required when the effluent concentration reaches half of the feed one (min)
u_0	linear flow rate of liquid phase (cm/h)

Greek letters

ε	bed void fraction
μ_L	viscosity of liquid phase (g/(cm s))
ρ_b	bed density (g/cm^3)
ρ_L	density of liquid phase (g/cm^3)
ρ_p	density of clay particle (g/cm^3)

(OPC): QASCs containing chlorophenols were solidified with OPC.

The isotherms and breakthrough characteristics are important for the evaluation of an adsorption process using organoclays. Although various models for sorption of metallic ions with organoclays [13–15] or activated carbon [16] have been used to predict column dynamics, not many studies have been done on the sorption of organic matter. Zhong and Meunier [17] studied the transport of organic contaminants in fixed beds containing aggregates of clay minerals and organic matter as sorbents using a two-region model. This model basically needs many parameters that are either determined by independent experiments or estimated by suitable correlations and sophisticated calculations. This makes the model rather inconvenient for practical use.

The aim of this study is to investigate the column performance of a new geomaterial, clay-active coal-coated cement (CACC), for the removal of phenols from an aqueous environment in a continuous flow system. Accurate scale-up data in fixed-bed systems cannot be obtained from the adsorption isotherms, so the practical applicability of CACC was ascertained in column operations. A more extensive investigation of the effect of organics and Na^+–clays on the hydratation kinetics, physico-mechanical properties and leaching behavior of cement-based solidified wastes is proposed.

Table 1a
Chemical composition and physicochemical properties of bentonite used

	Chemical composition (%)	
	Clay	Silice
SiO_2	58.5	94.8
Al_2O_3	19.5	1.2
Fe_2O_3	2.8	0.6
$CaCO_3$	1.2	3.2
MO	6.01	–
M_2O	4.3	–
H_2O	7.19	0.02

An attempt was made here to apply a simple model, i.e., the constant-pattern concept of wave propagation theory, to predict breakthrough dynamics [18,19]. Phenol, 2-NP, 2-CP and xylene were selected as the sorbates. The overall liquid-phase mass transfer coefficients were also determined by a constant-pattern wave approach and the effect of axial dispersion on the breakthrough characteristics was evaluated.

2. Materials and methods

2.1. Geomaterials

Montmorillonite (Maghnia bentonite obtained from Entreprise Nationale des Matiéres Non Férreux (ENOF, Algeria) was fractionated by allowing larger particles to settle out of suspension and collecting the <2.0 μm fraction. This fraction was used to prepare homoionic clay of Na-montmorillonite by washing the clay three times with a 1 M solution of NaCl. Excess salt was removed by washing the clay with distilled water until the supernatant was free of chlorides (<0.1 mM). The salt-free clay was freeze-dried and stored at room temperature. The homoionic clay had an idealized formula of $Al_2O_3{\cdot}4SiO_2{\cdot}nH_2O$. The cation exchange capacity of the raw clay was 70 mequiv/100 g. The BET surface area and mean pore size were measured to be, respectively, 90 m^2/g and 3.5 nm (Table 1a).

The active carbon used in the confection of these geomaterial is an activated wood coal with micoporous structure; the main characteristics are presented in Table 1b. The cement has been used for the elaboration of the geomaterial (it was from Chelf province in west of Algeria) with a proportion of SiO_2 (94.8%) of the global mass, all chemical and physical properties are shown in Table 1b.

Table 1b
Physicochemical properties of carbon and cement used

Main characteristics	Silice	Active carbon	Clay
S_{BET} (N_2/77 K)	12	950	90
Particle size (μm)	200–250	<20	<2
pH	5.8	3.5	6.5
Humidity (%)	2.5	7.8	9

Table 2
Some characteristics of prepared CACC geomaterial

Parameters	Geomaterial
S_{BET} (m^2/g)	220
V_p (cm^3/g)	0.153
Pt (%)	8.5
Density (g/cm^3)	1.18

2.2. Preparation of the geomaterials-modified clays

The geomaterial are prepared by assembly of several constituents: Na^+-montmorillonite, active charcoal, cement, and water 70%, 7%, 7% and 16% (w/w/w/w), respectively. Then, a mechanical mixing was carried out for 48 h at a moderate speed (40 tr/min). After a separation by centrifugation and a drying air we can obtain the final material.

These materials (clay-active coal-coated cement CACC), were chosen in order to associate the mechanical solidity due to the cement and a part of the clay to adsorption properties due to the active carbon and the clay mineral; some characteristics of CACC geomaterial are given in Table 2.

3. Sorption experiments

3.1. Batch sorption

For equilibrium sorption and to determine the isotherms, different masses (0.05–1 g) of air-dried goematerials were first added to 10 sealed batch flasks vessels, each filled with 50 ml aqueous solution with 20 ppm (~0.21, 0.18, 0.15 and 0.13 mol/m^3), respectively, for phenol, xylene, 2-CP and 2-NP. The analytical-grade reagents phenol, 2-NP, 2-CP, xylene, and other inorganic chemicals were supplied by Sigma–Aldrich Co. and their characteristics are shown in Table 3.

The initial pH of the aromatic solutions was preserved during adsorption experiments between 4.5 and 5 by adding a small volume of 0.1 M of HCl solution. The flasks were then shaken at 300 rpm and 25 °C in a temperature-controlled shaker for 24 h. After filtration with glass fiber and centrifugation at 2500 rpm,

Table 3
Molecular weight (M_W), pK_a [20] and solubility [21] of the models compounds

	Compound			
	Phenol	2-CP	2-NP	Xylene
Molecular mass (M_W)	94.11	128.56	139.11	108.14
Density	1.07	1.26	–	0.86
pK_a	9.89	8.48	7.15	–
Solubility at 20 °C (g/l)	90	15.5	16	20
λ_{max} (nm)	269	273.5	358	265
$pH_{initial}$	5.15	4.5	5.2	4.9
V (cm^3 mol^{-1}/100) (molecular volume) [25]	0.53	0.72	0.68	0.67
π (the polarity/polarizability parameter) [25]	0.72	0.75	1.11	0.51
log K_{ow}	1.46	2.15	1.83	3.26
Purity[a] (%)	99.0	99.0	99.0	99.0

[a] As received from Sigma–Aldrich Corporation, Spain.

Table 4
Characteristics of the column packed with goematerials-modified clay

Bed void fraction, ε	0.59
Bed density, ρ_b (g/ml)	0.637
Bed height, L (cm)	10
Particle size, d_p (μm)	~200–250
Particle density, ρ_p (g/ml)	1.18
Total length of the column (cm)	14

the concentrations of phenols and xylene after sorption were analyzed at λ_{max} (Table 3) using a UV spectrometer (Shumadzu) model. The amounts of phenols sorbed onto the clay and at equilibrium, q (mmol/g), were calculated from the mass balance relation:

$$q = \frac{V}{W}(C_0 - C_e) \quad (1)$$

Each run was performed at least twice under identical conditions. The reproducibility of the measurements was mostly within 3%.

3.2. Column experiments

Fixed-bed tests were carried out in a water-jacketed glass column with an internal diameter of 1.25 cm and a length of 14 cm. The bed density and void fraction were determined prior to the experiment, all the experimental conditions and calculated results of the four column tests are summarized in Table 4.

The aqueous solution with a sorbate concentration of 20 ppm and at solution pH (4.5–5) was continuously feed to the top of the column at a desired (~0.5 m^3/[m^2 h]) flow rate controlled by a peristaltic pump (Cole-Parmer) until the breakthrough curve occurred, after for 5 days of adsorption, the higher pH raise occurred 10 U. The effluent samples were taken at the present time intervals and their concentrations were analyzed as described above by a UV-spectrophotometer (M40-Shumadzu) model at their λ_{max} (Table 3).

4. Model development

We consider for an isothermal fixed bed packed randomly with sorbent particles, the governing equation for predicting column dynamics is [22,23]:

$$\varepsilon\left(\frac{\partial C}{\partial t}\right) + u_0\varepsilon\left(\frac{\partial C}{\partial z}\right) + \rho_b\left(\frac{\partial q}{\partial t}\right) = 0 \quad (2)$$

where ε is the bed void fraction, ρ_b the bed density, u_0 the interstitial flow rate, t the contact time, z the distance from the inlet of the bed, and C and q are the sorbate concentrations in liquid and solid phases, respectively. Basically, Eq. (2) is the unsteady-state mass balance for the sorbate. The assumptions associated with Eq. (3) include the following:

- No chemical reactions occur in the column.
- The flow pattern is the ideal plug flow.
- Only mass transfer by convection is significant.
- Radial and axial dispersions are negligible.
- The flow rate is constant and invariant with column position.

The sorption rate of sorbate within the particles can be simply described by the linear driving force model in terms of the overall liquid-phase mass transfer coefficient $K_L a$ [24] where K_L is the overall liquid-phase mass transfer coefficient, a the contact area per unit bed volume, and C_e is the liquid-phase concentration in equilibrium with solid-phase concentration q. The liquid- and solid-phase concentrations are related by the generalized sorption isotherm:

$$\rho_b \left(\frac{\partial q}{\partial t}\right) = \varepsilon K_L a (C - C_e) \tag{3}$$

$$C_e = f(q) \tag{4}$$

The propagation theory of constant-pattern waves moving at a constant flow rate, u_c was adopted in this study [23]. The liquid-phase concentration can be expressed as a unique function of the adjusted time t, defined as

$$\tau = t - \frac{z}{u_c} \tag{5}$$

Substitution of Eq. (5) into Eq. (2) leads to

$$\left(1 - \frac{u_0}{u_c}\right)\left(\frac{dC}{d\tau}\right) + \left(\frac{\rho_b}{\varepsilon}\right)\left(\frac{dq}{d\tau}\right) = 0 \tag{6}$$

Eq. (6) can be integrated as

$$\left(1 - \frac{u_0}{u_c}\right) C + \left(\frac{\rho_b}{\varepsilon}\right) q = 0 \tag{7}$$

As the boundary condition ($q = q_F$) at ($C = C_F$) is satisfied, the following equation holds:

$$\left(1 - \frac{u_0}{u_c}\right) C_F + \left(\frac{\rho_b}{\varepsilon}\right) q_F = 0 \tag{8}$$

where C_F is the feed sorbate concentration in the liquid phase and q_F is its associated equilibrium concentration in solid phase. Combining Eqs. (7) and (8), we have

$$\left(\frac{q}{C}\right) = \left(\frac{q_F}{C_F}\right) \tag{9}$$

Eq. (9) is the keystone for deriving breakthrough curves of column operations. The sorption rate within the particles expressed in terms of the adjusted time t is

$$\rho_b \left(\frac{\partial q}{\partial \tau}\right) = \varepsilon K_L a (C - C_e) \tag{10}$$

Combining Eqs. (9) and (10), we obtain:

$$\rho_b \left(\frac{q_F}{C_F}\right)\left(\frac{dC}{d\tau}\right) = \varepsilon K_L a (C - C_e) \tag{11}$$

Replacement of the liquid-phase equilibrium concentration C_e by $f((q_F C)/C_F)$ and combination with Eq. (9) leads to

$$\rho_b \left(\frac{q_F}{C_F}\right)\left(\frac{dC}{d\tau}\right) = \varepsilon K_L a \left(C - f\left(q_F \frac{C}{C_F}\right)\right) \tag{12}$$

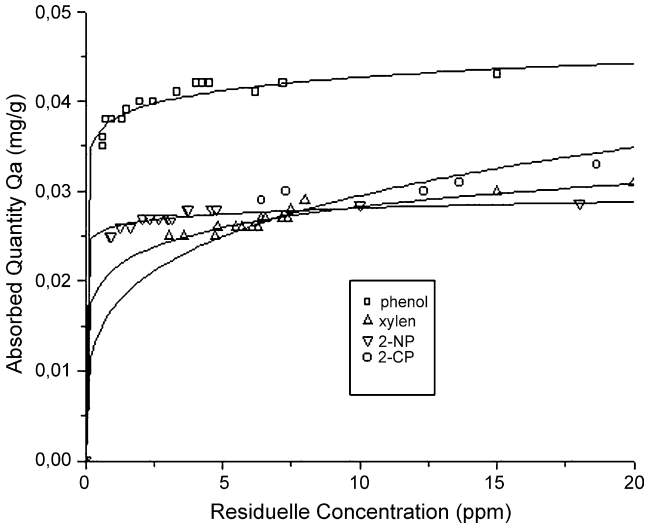

Fig. 1. Sorption isotherms of phenols onto (CACC) geomaterials at 25 °C: symbols represent experimental data and the solid line is the Langmuir model.

Eq. (12) can be rearranged and integrated with the boundary condition ($C = C_F/2$) at $\tau = \tau_{1/2}$, and the form becomes:

$$\tau = \tau_{1/2} + \frac{\rho_b q_F}{\varepsilon K_L a C_F} \int_{C_F/2}^{C} \frac{1}{C - f(q_F C / C_F)}\, dC \tag{13}$$

It is assumed that $K_L a$ is kept constant. Since $(\tau - \tau_{1/2}) = (t - t_{1/2})$ from Eq. (5), the breakthrough curve at $z = L$ can be calculated by the following equation:

$$t = t_{1/2} + \frac{\rho_b q_F}{\varepsilon K_L a C_F} \int_{C_F/2}^{C} \frac{1}{C - f(q_F C / C_F)}\, dC \tag{14}$$

5. Results and discussion

5.1. Sorption isotherms

Fig. 1 shows the sorption isotherms, which can be fitted by the Langmuir equation obeying the thermodynamic condition of Henry's law over an infinitely dilute concentration range [21]:

$$q = \frac{q_m K_l C_e}{1 + K_l C_e} \tag{15}$$

where q_m is the monolayer sorption capacity and K_l is the Langmuir constant. The linear plot of $1/q$ versus $1/C_e$ gives the values of q_m and K_l, which are listed in Table 5. The fitting is good (determination coefficient $R^2 \geq 0.99$). The sorption capacity q_m decreases in the order phenol > xylene > 2-NP > 2-CP. This could be correlated to their water solubilities (g/100 g H_2O), which are

Table 5
Parameters for the Langmuir equation

Sorbate	K_l (mM^{-1})	q_m (mmol/g)
Phenol	0.67	0.458
2-NP	1.01	0.326
2-CP	0.12	0.206
Xylene	0.101	0.35

9.0, 2.0, 1.6, and 1.55, respectively, for phenol, xylene, 2-NP and 2-CP (Table 3).

Generally, adsorption depends on the electric charge of the pollutants. The pollutants can be adsorbed by ionic, polar, hydrophobic or hydrophilic interactions.

Where steam pressures are low in the case of compounds with high molecular weights, their octanol–water (K_{ow}) were higher. The effect of internal hydrogen bonding leads to remarkable changes in hydrophobicity. If $\log K_{ow}$ is used as an index of hydrophobicity, the order of increasing $\log K_{ow}$ value is phenol < 2-NP < 2-CP < xylene (Table 3) [25].

The general indications from the solvation model are that dispersion interactions are the most important for retention on sorbents. These interactions are reinforced by polar interactions due to dipole/polarization and lone pair electron attraction. In this way, we can note that π^* parameter values (Table 3) decrease $\pi^*_{xylene} < \pi^*_{phenol} < \pi^*_{2\text{-CP}} < \pi^*_{2\text{-NP}}$ with the opposite order of the adsorption capacity except for xylene.

The solvophobic effects of aqueous solutions are important, as they always are when water is the major component of the solvent/mobile phase. The main comparative of the compounds molar volume (Table 3), we can observe that their values increase in opposite order of adsorption capacity and the order become $V_{2\text{-CP}} > V_{2\text{-NP}} > V_{xylene} > V_{phenol}$.

The steric hindrance factor is also more significant in this system as phenol has the least steric effect and smallest molecular size. These results agree with those obtained previously [26,27]. For example, Juang et al. [28] found that sorption capacity (in g/kg) onto the CTAB-montmorillonite decreases in the order *m*-NP > *o*-cresol > phenol. The order becomes phenol > *m*-xylene > 2-CP > 2-NP in the present study if the capacity is expressed in (mmol/g).

We can explain the difference in sorption capacity mainly by the van der Waals interaction between sorbate and active site of adsorbent, originating from the difference in water solubility and acidity of the sorbate. Obviously the answers to these questions require further investigation concerning the intermolecular interactions.

5.2. Breakthrough dynamics

A typical breakthrough curve is obtained by plotting the phenols' (phenol, 2-NP, 2-CP) and *m*-xylene ratio concentrations (C/C_F) against time (in h), as shown in Fig. 2. The break point for phenol appears faster than those for 2-NP, 2-CP and *m*-xylene, as the amount of sorption (not the monolayer capacity) of phenol is smallest under this condition ($C_F = 0.206$ mM). Initially, all the phenols and xylene were adsorbed resulting in zero solute concentration in the effluent. As the column operation continues, the lower layers of the adsorbent become saturated with phenols and the adsorption zone progresses upward through the CACC beds. Eventually, the adsorption zone reaches the top of the column and the phenols' concentrations in the effluent begin to increase.

The breakthrough curves for the phenols and xylene where obtain for the same bed depths (10 cm) and a flow rate of ($F_r = 0.6$ ml/min (~0.5 $m^3/[m^2\ h]$).

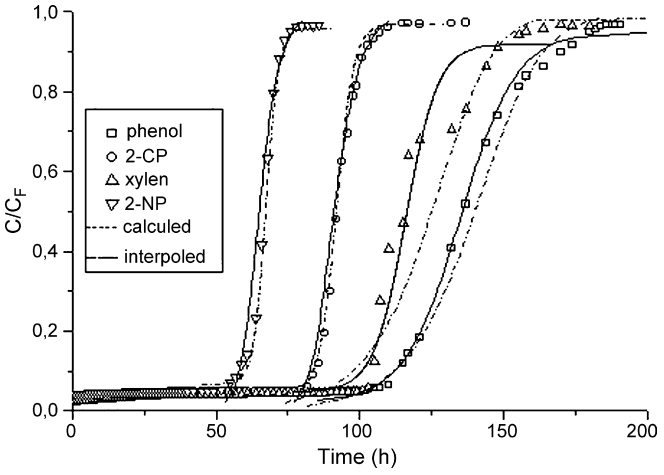

Fig. 2. Breakthrough curves of phenols using (CACC) geomaterials.

The point on the breakthrough curve at which the phenols concentration reaches its maximal permissible value (0.1 ppm) is referred to as the breakthrough.

The breakthrough times which corresponding to ($C/C_0 = 0$, 5%) for 2-NP, 2-CP, xylene and phenol were found to be 50.5, 71, 100.5 and 101.5 h, respectively. The point where the phenol's concentration reaches 95% of the influent value (20 ppm) is called the point of column exhaustion.

The exhaustion times were 54, 97.5, 130 and 176 h, respectively, for 2-NP, 2-CP, xylene and phenol; combination of Eqs. (14) and (15) leads to

$$t = t_{1/2} + \left(\frac{\rho_b q_F}{\varepsilon K_L a C_F}\right)\left[\ln 2x + \left(\frac{1}{1 + K_1 C_F}\right)\ln\left(\frac{1}{2(1-x)}\right)\right] \quad (16)$$

where x is the normalized effluent concentration ($=C/C_F$). The applicability of Eq. (16) is justified by the linear plot as shown in Fig. 3. In this regard, the values of $t_{1/2}$ and $K_L a$ are obtained from the intercept and slope of the linear plot with $r^2 > 95$, allowing the estimation of the parameter $t_{1/2}$, listed in Table 6. It can be observed that there is a good fit of the model equation to exper-

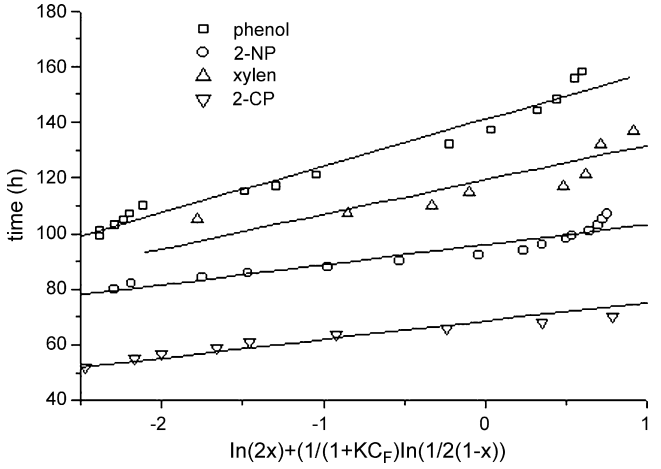

Fig. 3. Validity of the constant-pattern wave model.

Table 6
Parameters of constant-pattern wave model for phenols at operating feed flow rates

Sorbate	Flow rate, u_0 (cm/h)	$t_{1/2}$ (h)	$K_L a$ (h^{-1})
Phenol	45.8	146.32	39.25
2-NP	45.8	90.97	2.99
2-CP	45.8	64.01	0.35
Xylene	45.8	130.72	31.17

imental data under the operating conditions, which assumes an ideal plug flow behavior that implies symmetrical breakthrough curves, this only predicts satisfactorily the breakthrough curves for $t_{op} \leq t_{1/2}$ (were t_{op} is the operating time).

The solid curves shown in Fig. 2 are calculated from Eq. (16), indicating good agreement with the experimental results. It is evident that the value of $t_{1/2}$ for 2-CP, 2-NP and *m*-xylene is not larger than that of phenol. The similar halftime $t_{1/2}$ for 2-NP and *m*-xylene is probably due to equivalent amounts of sorption on the CACC geomaterials-modified clay at phenols feed (C_F) as shown in Fig. 1. Axial dispersion (D_L) is one of the mechanisms responsible for the broadening of concentration profiles in fixed-bed adsorbers and, therefore, it has been taken into account in the modeling of the breakthrough curves obtained at the low flow rates.

For evaluating the contribution of axial dispersion, the following equation is adopted if the Langmuir equation is involved [26]:

$$P_{eB}\left(1-\frac{\tau}{\delta}\right) = \left(\frac{1}{1-\alpha}\right)\ln\left[\frac{1-C/C_F}{(C/C_F)^{\alpha}}\right] \quad (17)$$

where $P_{eB} = (u_0 L/D_L)$, $\tau = (tu_0/L)$, $\partial = (\rho_b q_F(1-\varepsilon)/\varepsilon C_F)$ and $\alpha = 1/(1+K_1 C_F)$.

If axial dispersion predominates, the plot of $[1-(\tau/\delta)]$ versus $\ln[(1-C/C_F)/(C/C_F)^{\alpha}]$ gives a straight line with zero intercept. This is not the case due to the positive intercept (Fig. 4). This confirms the validity of Assumption 4 as indicated above. The axial

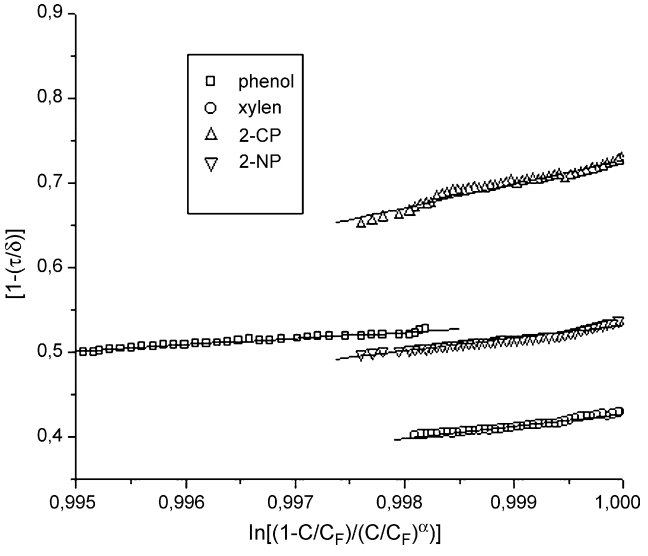

Fig. 4. Contribution of the axial dispersion effect.

Table 7
The measured overall mass transfer coefficient and calculated individual liquid-film mass transfer coefficient

Sorbate	Flow rate, u_0 (cm/h)	Measured $K_L a$ (h^{-1})	Calculated $k_L a$ (h^{-1})	$Pe^{+3}_{B.10}$	D_L (cm^2/h)
Phenol	45.8	39.2	39.04	166	2.75
2-NP	45.8	2.99	63.9	79.6	5.75
2-CP	45.8	0.35	91.6	46.6	9.82
Xylene	45.8	31.1	62.3	81.6	5.61

Bed height = 10 cm, bed void fraction = 0.5, $C_F = \sim 0.21$, 0.18, 0.15 and 0.13 mol/m^3, respectively, for phenol, xylene, 2-CP and 2-NP.

dispersion coefficient, D_L, is affected by molecular diffusion and by the dispersion related to fluid flow; thus, this parameter is expected to increase with increasing compound solubility, as is the case for the experiments.

The following correlation, suggested by Suzuki [22], is used to predict individual liquid-film mass transfer coefficients k_L in the range $0.0015 < Re < 55$:

$$Sh = \left(\frac{1.09}{\varepsilon}\right) Sc^{1/3} Re^{1/3} \quad (18)$$

where $Sh = k_L d_p/D_L$, $Re = \rho_L u_0 \varepsilon d_p/\mu_L$, and $Sc = \mu_L/\rho_L D_L$. Calculating k_L by Eq. (18) and the contact area per unit bed volume by $a = 6(1-\varepsilon)/d_p$.

We find that calculated $K_L a$ (Table 7) is higher than measured $K_L a$. This possibly implies that solid-phase mass transfer resistance exists and plays a certain role in the breakthrough dynamics.

It is likely that the driving force for mass transfer becomes no greater when the phenols' solubility is increased at a given bed height. The overall liquid-phase mass transfer coefficient K_L generally contains the individual liquid-film mass transfer coefficient and convective mass transfer coefficient. In this study, the increased $K_L a$ value with increasing phenol solubility (phenol > xylene > 2-NP > 2-CP) is likely attributable to the decreased resistance of liquid-film diffusion as the dependence of convective mass transfer on solubility is comparatively significant.

A higher bed represents a larger amount of the sorbent. Hence, the driving force for mass transfer will discount at a given C_F. This will be an important step for the wider use of CACC materials and to study the effect of bed height on the $K_L a$ value. To make further progress, emphasis should be placed on the creation of large data sets for varied solutes and different solvents, so that the capacity of CACC for intermolecular interactions can be delineated more succinctly and the varied aspects of retention mechanisms quantified and understood.

5.3. Determination of dynamic capacity and unused bed length (LUB)

Once the breakthrough time (t_{bt}) was determined, the dynamic capacity of the CACC (Q_{dc}), i.e., the amount of phenols adsorbed on the CACC at the breakpoint, was calculated (Table 8) as: Q_{dc} (mg of phenols adsorbed/g of CACC) = $[(C_F - C)F_r t_{bt}/m]$ where C and C_F are the outlet and

Table 8
Experimental breakthrough time, dynamic capacity of the CACC and equivalent length of unused beds (LUB) for phenols operating conditions

Compounds	t_{bt} (h)	Q_{dc} (mg phenols/g CACC)	LUB (cm)
Phenol	101.5	13.7	8.32
Xylene	100.5	13.72	8.49
2-CP	71	9.62	8.61
2-NP	50.5	6.81	8.63

inlet phenols' concentrations, respectively, F_r the flow rate of the aqueous phenols' solutions and m is the weight of CACC.

It can observe that under the operating conditions, the capacity is independent of the solubility of the phenol compounds, however, an increase in the t_{bt} between 2-NP and 2-CP or 2-CP and xylene, implied an increase in the dynamic capacity of approximately 30% (Table 8). Apart from the breakthrough time of a bed of specified height, another parameter for the design of an adsorber is the equivalent length of unused bed (LUB), which can be obtained by analysis of the breakthrough curves according to

$$\mathrm{LUB} = \left(1 - \frac{Q_{dc}}{Q_{sat}}\right) L = \left(1 - \frac{t_{bt}}{t*}\right) L = \int_0^\infty \left(1 - \frac{C}{C_F}\right) \mathrm{d}t \tag{19}$$

where L is the bed length, t^* the stoichiometric time and Q_{sat} is the adsorbed phenols at the bed saturation. This is used to determine the length of a full-scale adsorbent bed as the sum of the length of the ideal fixed-bed adsorber (LES), i.e., the stoichiometric length of bed needed to produce the desired adsorption capacity of the bed, based on ideal step-function behavior, plus the LUB, as additional length. The LUB design approach assumes that the adsorption bed is long enough to produce constant-pattern behavior and that the system is governed by a convex isotherm. The LUB was determined from the breakthrough curves, obtaining the results shown in (Table 8). Thus, the percentages of the adsorption capacity used at the breakthrough time were approximately 83–86%.

6. Conclusions

In this study, an extensive laboratory investigation was carried out to evaluate the fixed-bed column performance of a re-usable sorbent (removal by adsorption). This new adsorbent, termed clay-active coal-coated cement (CACC), was found to be very effective in removing phenols from aqueous solution. The breakthrough curves for sorption of phenol, 2-NP, 2-CP and *m*-xylene using CACC geomaterials, modified montmorillonite, were measured. Two important parameters involved in this model, $t_{1/2}$ and K_La, were directly and simply determined by Eq. (16) and were related to the system constant such as the feed flow rate (45.8 cm/h) and feed sorbate concentration ($C_F = \sim 0.21, 0.18, 0.15$ and $0.13\ \mathrm{mol/m^3}$). The constant-pattern wave approach with the Langmuir equation well predicted breakthrough dynamics. The contribution of axial dispersion is expected to increase with increasing compound solubility in these systems. The operating conditions, produced an increase in $t_{1/2}$ and measured K_La, in the same sequence as their solubilities (phenol > xylene > 2-NP > 2-CP). The present study has provided a simple and easy-to-follow method for analyzing the breakthrough characteristics for the sorption of organic matter on geomaterials–clays.

References

[1] C.M. Castilla, Adsorption of organic molecules from aqueous solutions on carbon materials, Carbon 42 (2004) 83–94.
[2] M.S. El-Shahawi, H.A. Nassif, Kinetics and retention characteristics of some nitrophenols onto polyurethane foams, Anal. Chim. Acta 487 (2003) 249–259.
[3] C. Namasivayam, D. Kaitha, Adsorptive removal of 2-chlorophenol by low-cost coir pith carbon, J. Hazard. Mater. 98 (2003) 257–274.
[4] Z. Yaneva, B. Koumanova, Comparative modeling of mono- and dinitrophenols sorption on yellow bentonite from aqueous solutions, J. Colloid Interf. Sci. 293 (2006) 303–311.
[5] O. Bouras, M. Houari, H. Khalaf, Adsorption of some phenolic derivatives by surfactant treated Al-pillared Algerian bentonite, Toxicol. Environ. Chem. 70 (1999) 221–227.
[6] O. Bouras, M. Houari, H. Khalaf, Using of surfactants modified Fe-pillared bentonite for removal of pentachlorophenol from aqueous stream, Environ. Technol. 22 (2001) 69–74.
[7] D.M. Montgomery, C.J. Sollars, R. Perry, Optimization of cement-based stabilization/solidification of organic-containing industrial wastes using organophilic clays, Waste Manage. Res. 9 (1991) 21–34.
[8] V.M. Hebatpuria, H.A. Arafat, P.L. Bishop, N.G. Pinto, Immobilization of phenol in cement-based solidified/stabilized hazardous wastes using regenerated activated carbon: leaching studies, J. Hazard. Mater. 70 (1999) 117–138.
[9] G.W. Beall, Organic waste disposal, US Patent no. 4473477 (1984).
[10] G.W. Beall, Method of immobilizing organic contaminants to form of non-flowable matrix, US Patent no. 4650590 (1987).
[11] K.S. Jun, H.S. Shin, B.C. Paik, Microstructural analysis of OPC/silical fume/Na-bentonite interaction in cement based solidification of organic contamined hazardous waste, J. Environ. Sci. Health, Part A: Environ. Sci. Eng. Toxicol. 4 (1999) 913–918.
[12] D.M. Montgomery, C.J. Sollars, R. Perry, S.E. Tarling, P. Barnes, E. Henderson, Treatment of organic-contamined industrial wastes using cement-based stabilisation/solidification, Waste Manage. Res. 9 (1991) 113–125.
[13] J.H. Yun, D.K. Choi, H. Moon, Benzene adsorption and hot purge regeneration in activated carbon beds, Chem. Eng. Sci. 55 (2000) 5857–5872.
[14] J.A. Berninger, R.D. Whitley, X. Zhang, N.-H.L. Wang, A versatile model for simulation of reaction and nonequilibrium dynamics in multicomponent fixed-bed adsorption process, Comput. Chem. Eng. 15 (1991) 749–768.
[15] G.M. Zhong, F. Meunier, Linear perturbation chromatography theory: moment solution for two-component nonequilibrium adsorption, Chem. Eng. Sci. 48 (1993) 1309–1315.
[16] M. Baudu, P. Le Cloirec, G. Martin, Pollutant adsorption onto activated carbon membranes, Water Sci. Technol. 23 (1991) 1659–1666.
[17] G.M. Zhong, F. Meunier, Interference theory. Part I. Moment solution for two-component nonequilibrium adsorption chromatography, Chem. Eng. Sci. 48 (1993) 4105–4108.
[18] T. Vermeulen, in: T.B. Drew, J.W. Hoopes Jr. (Eds.), Advances in Chemical Engineering, Academic Press, New York, 1958.
[19] U.K. Traegner, M.T. Suidan, B.R. Kim, Considering age and size distributions of activated-carbon particles in a completely-mixed absorber at steady state, Water Res. 30 (1996) 1495–1501.
[20] D. Lide, CRC Handbook of Chemistry and Physics: A Ready-Reference Book of Chemical and Physical Data, CRC Press, Boca Raton, 2003.
[21] Sigma–Aldrich Corporation, Material Safety Data Sheets, Sigma–Aldrich Corporation, Spain, 2003.
[22] M. Suzuki, Adsorption Engineering, Elsevier, Amsterdam, 1989.

[23] J.M. Chem, Y.W. Chein, Adsorption of nitrophenol onto activated carbon: isotherms and breakthrough curves, Water Res. 36 (2002) 647–655.
[24] T.K. Sherwood, R.L. Pigford, C.R. Wilke, Mass Transfer, McGraw-Hill, New York, 1975.
[25] D.C. Luehrs, et al., Linear solvation energy relationship of the limiting partition coefficient of organic solutes between water and activated carbon, Environ. Sci. Technol. 30 (1996) 143–152.
[26] M.A.M. Lawrence, R.K. Kukkadapu, S.A. Boyd, Adsorption of phenol and chlorinated phenols from aqueous solution by tetramethylammonium and tetramethylphosphonium-exchanged montmorillonite, Appl. Clay Sci. 13 (1998) 13–20.
[27] B.C. Pan, P.W. Meng, et al., Application of an effective method in predicting breakthrough curves of fixed bed adsorption onto resin adsorbent, J. Hazard. Mater. B124 (2005) 74–80.
[28] R.S. Juang, et al., Sorption of phenols from water in column systems using surfactant-modified montmorillonite, J. Colloid Interf. Sci. 269 (2004) 46–52.